A novel composite adsorbent coated superhydrophilic-nanostructured heterogeneous surface for condensation heat transfer enhancement

Chen, Siru; Pan, Aiqiang; Zhu, Yihao; Ho, Tsz Chung; Lee, Hau Him; Zeng, Yijun; Wu, Chili; Qiu, Huihe; Tso, Chi Yan

Published in:
International Journal of Thermal Sciences

Published: 01/02/2023

Published version (DOI):
10.1016/j.ijthermalsci.2022.107978

Publication details:
Chen, S., Pan, A., Zhu, Y., Ho, T. C., Lee, H. H., Zeng, Y., Wu, C., Qiu, H., & Tso, C. Y. (2023). A novel composite adsorbent coated superhydrophilic-nanostructured heterogeneous surface for condensation heat transfer enhancement. *International Journal of Thermal Sciences*, *184*, Article 107978. https://doi.org/10.1016/j.ijthermalsci.2022.107978

A Novel Composite Adsorbent Coated Superhydrophilic-Nanostructured Heterogeneous Surface for Condensation Heat Transfer Enhancement

Siru Chen[1], Aiqiang Pan[1], Yihao Zhu[1], Tsz Chung Ho[1], Hau Him Lee[1], Yijun Zeng[2], Chili Wu[3], Huihe Qiu[3], Chi Yan Tso[1,*]

[1] School of Energy and Environment, City University of Hong Kong, Hong Kong

[2] Department of Mechanical Engineering, City University of Hong Kong, Hong Kong

[3] Department of Mechanical and Aerospace Engineering, The Hong Kong University of Science and Technology, Clear Water Bay, Hong Kong, China

* Corresponding Author Tel.: +852 3442 4623; Fax: +852 3442 0688

E-mail Address: chiytso@cityu.edu.hk

Postal Address: School of Energy and Environment, City University of Hong Kong, 83 Tat Chee Ave, Kowloon Tong, Kowloon, Hong Kong

Highlights

- Heterogeneous surfaces formed by adsorbents and superhydrophilic coatings;
- Condensation heat transfer evaluation of various heterogeneous surfaces;
- Critical improvement in latent heat transfer achieved by heterogeneous surfaces;
- Water film adsorption mechanism is introduced to explain enhanced condensation.

* Corresponding author: chiytso@cityu.edu.hk; Tel.: +852 3442 4623

Abstract

In this work, a novel composite adsorbent coated superhydrophilic-nanostructured heterogeneous surface is proposed to enhance condensation heat transfer. Experiments are conducted under the atmospheric pressure condition with the ambient temperature of 23 ± 2 °C to investigate the water vapor condensation rate of the heterogeneous surfaces coated with different patterns of the composite adsorbent. The condensation rates and the latent heat transfer coefficients of the heterogeneous surfaces are investigated under the quiescent environment. The results show that the heterogeneous surfaces with vertical middle-stripe patterns of the composite adsorbent have better condensation heat transfer performance than the other patterns, showing 45.5% to 80.0% improvement compared to the copper surface. It is found that during water condensation on the heterogeneous surfaces, the water film on the superhydrophilic region can be adsorbed by the adjacent composite adsorbent. Consequently, a water-free region is observed on the proposed heterogeneous surfaces, which provides extra fresh nucleation sites for water condensation, leading to an enhancement in the heat transfer performance. Based on this observation, a water film adsorption mechanism is introduced to explain the condensation heat transfer enhancement on the proposed heterogeneous surface, providing a practical and scalable surface treatment method to improve the condensation heat transfer.

Keywords: Adsorbents; Condensation; Heat Transfer; Nanostructured Surfaces; Superhydrophilicity.

Nomenclature

$\dot{m}_w$	Condensation rate ($kg/m^2 \cdot min$)
h_{fg}	Latent heat of evaporation (kJ/kg)
C_{LTH}	Latent heat transfer coefficient ($W/m^2 \cdot K$)
T_{dew}	Dew point temperature ($℃$)
T_s	Substrate temperature ($℃$)
T_∞	Ambient temperature ($℃$)
θ	Contact angle (°)
AAR	Composite adsorbent area ratio (%)
MAR	Composite adsorbent mass area ratio (g/m^2)
Bo	Bond number

1. Introduction

Water vapor condensation is a ubiquitous phenomenon in various heat transfer applications when the surface temperature is lower than the dew point temperature , such as air conditioning systems [1, 2], water harvesting systems [3, 4], desalination systems [5, 6], air dehumidification systems [7], and thermal management systems [8]. The performance of these thermal applications is directly associated with the condensation heat transfer performance of heat exchangers. Therefore, improving the condensation heat transfer performance on the heat transfer surfaces is a practical approach to improve the overall system performance of these thermal applications.

Basically, surface condensation mainly takes two forms: filmwise condensation (i.e., thin liquid film is formed on the cooling surface) and dropwise condensation (i.e., droplets are formed on the cooling surface), corresponding to high surface wettability and low surface wettability respectively. According to the static contact angles of droplets on surfaces with different wettability, surfaces can be classified into superhydrophilic surfaces ($\theta < 10°$), hydrophilic surfaces ($\theta < 90°$), hydrophobic surfaces ($\theta > 90°$), and superhydrophobic surfaces ($\theta > 150°$) [9]. In general, dropwise condensation shows higher condensation heat transfer performance since in filmwise condensation, a liquid film is formed posing high thermal resistance between the surface and vapor, while droplets formed in dropwise condensation are removed from the surface.

Much research has been conducted to promote dropwise condensation by modifying surfaces, including low surface energy surfaces and micro/nano-structured surfaces, hydrophobic or superhydrophobic surfaces [10, 11]. The methods employed by many researchers to reduce surface free energy include metallization [12], ion implantation [13, 14], and polymer coatings [15]. However, these methods have disadvantages in the aspects of high cost, damage to surface, and life duration. Regarding the micro/nano-structured surfaces, various nanostructures have been fabricated on surfaces, including nanowires [16], nano-cones [17], nano-rods [18], nano-sheets [19], and nano-blocks [20], to increase the surface hydrophobicity and contact angle.

Although many studies have focused on promoting dropwise condensation, it does not necessarily lead to enhanced condensation heat transfer performance [11]. It should be noted that the removal of droplets is closely related to the two different droplet morphologies on the

hydrophobic surface, i.e., the Wenzel state [21] and Cassie state [22] droplet morphologies. Miljkovic et al. indicated that when the droplets condensed on the surface are in the Wenzel state, the removal of droplets is not fast enough, resulting in reduced heat transfer performance as described earlier, therefore realizing dropwise condensation does not necessarily lead to enhanced condensation heat transfer performance [23].

Regarding this, different types of composite surfaces have been proposed to enhance the condensation heat transfer. One type of composite surface is the patterned hydrophobic-hydrophilic surface [24-30]. In this type of patterned surface, hydrophilic stripes or grooves with different widths serve as drainage channels for the droplets condensed on the hydrophobic region, limiting the droplet size and renewing the hydrophobic region for new dropwise condensation, resulting in an improved condensation heat transfer coefficient. Similarly, a composite surface is proposed [31] with the wettability-patterned superhydrophilic tracks on a hydrophilic surface, making use of the capillary-driven condensate drainage from the superhydrophilic region to reduce the droplet size on the hydrophilic regions, thereby enhancing the dropwise condensation heat transfer of the surface. Another type of composite surface is the hydrophobic surface with micro-nano hydrophilic spots or sites [32-37]. The hydrophilic sites are used to control the nucleation on the hydrophobic surfaces, accelerating droplet growth rate, suppressing the droplet morphology of the Wenzel state, and promoting coalescence-induced droplet removal, hence, enhancing the condensation heat transfer performance [32-37]. For example, Zhu et al. improved the heat transfer coefficient of tube surfaces by using biphilic surfaces [33]. The hydrophilic sites are electrostatically coated on the superhydrophobic surface to form the biphilic surface. The convective heat transfer coefficient of the tube coated with the biphilic surface is improved by 29% and 38% in comparison with a typical copper tube and a tube with a superhydrophobic surface, respectively. Correspondingly, the condensation performance of the tube with the biphilic surface is enhanced by 123% as compared with that of a typical copper tube.

It should be noted that the studies of condensation heat transfer enhancement mentioned above are mainly based on dropwise condensation. Concerning filmwise condensation, the condensation heat transfer can also be improved by applying a porous layer on the condensation surface [38-41]. Wang et al. achieved a high heat transfer coefficient of the surface by applying a porous wick structure. Due to the capillary forces in the porous wick with high thermal

conductivity, the condensate in the porous wick can be quickly removed, substantially improving the heat transfer coefficient and condensation performance [39]. Preston et al. enhanced condensation heat transfer of the surface by having a porous metal wick on the condensation wall. Taking advantage of the condensate's affinity to the wet wick, gravitationally driven flow is developed in the porous metal wick, so that the water film is confined in the wet wick and efficiently removed from the surface. The wick filled with condensate has a lower thermal resistance than that of filmwise condensation, leading to an enhanced heat transfer coefficient of the wicking condensation [40]. Oh et al. developed a nanostructured superhydrophilic porous layer to enhance the condensation heat transfer [41]. Specifically, the thin superhydrophilic porous layer confines the condensate in the thin layer, forming thin-film condensation. It is reported that the heat transfer coefficient of thin-film condensation can approach as high as 100 $kW/K \cdot m^2$. However, the fabrication of such a porous structure is quite challenging and applying that structure on existing surfaces of heat exchangers is impractical, limiting wide application of this method.

In this study, a novel heterogeneous surface combining a composite adsorbent and superhydrophilic-nanostructured coating is proposed to efficiently enhance the condensation heat transfer coefficient of the filmwise condensation surface. On one hand, the porous composite adsorbent coating is similar to the porous layers that are used by different researchers to enhance the condensation heat transfer [38-41]. On the other hand, the porous composite adsorbent also has high adsorption ability of water vapor, accelerating the movement of the water vapor towards the surface, hence contributing to the condensation process. The porous composite adsorbent used in this work is multi-wall carbon nanotube (MWCNT)-embedded zeolite 13X/$CaCl_2$ composite adsorbent. Zeolite 13X molecular sieves are crystalline microporous structures with uniformly sized pores of molecular dimensions, which have a high affinity for moisture [42, 43]. The high water vapor adsorption ability and the high thermal conductivity of the MWCNT-embedded zeolite 13X/$CaCl_2$ composite adsorbent with a porous structure is believed to be able to enhance the condensation heat transfer. An effective self-assembly chemical method is utilized to fabricate the superhydrophilic-nanostructured surface, whose filmwise condensation mechanism (with high surface energy) facilitates good contact between the composite adsorbent and the condensate, allowing a smooth adsorption process of condensate from the superhydrophilic surface to the adsorbent. In addition, different

patterns of the composite adsorbents are coated on a superhydrophilic-nanostructured surface to study their condensation heat transfer performance.

This study proposes a novel composite adsorbent coated superhydrophilic-nanostructured heterogeneous surface which can efficiently enhance condensation heat transfer. The water film adsorption mechanism is firstly introduced to explain the enhancement of the condensation heat transfer performance. The condensation experiments, i.e., water collection experiments, are conducted under different relative humidity levels and substrate temperatures to compare the condensation heat transfer performance among different surfaces (i.e., different composite adsorbent patterns coated on heterogeneous surfaces, untreated copper surface and the pure superhydrophilic-nanostructured surface). The condensation experimental results are then compared and discussed comprehensively to demonstrate the condensation heat transfer enhancement of the novel heterogeneous surface (i.e., composite adsorbent coated superhydrophilic-nanostructured heterogeneous surface). For the first time, a water film adsorption mechanism for enhancing the condensation heat transfer of filmwise condensation by using the composite adsorbent is introduced. Most importantly, the strategy proposed in this study has the potential of wide application since the fabrication process is scalable and existing heat exchangers can be easily modified to improve the condensation heat transfer performance.

2. Materials and Methods

2.1 Composite adsorbent coated superhydrophilic-nanostructured heterogeneous surfaces preparation

As shown in Figure 1, there are three main steps to fabricate the novel heterogeneous surface. The first step is to prepare and synthesize the composite adsorbent, i.e., MWCNT-embedded zeolite 13X/$CaCl_2$ as shown in Figure 1(a). In Figure 1(b), the second step is to fabricate the nano-scaled superhydrophilic layer on a flat copper surface via a self-assembly chemical method reaction, one of the most cost-effective and time-saving ways to coat the nanostructure on the substrate [40, 41]. As shown in Figure 1(c), the third step is to coat the composite adsorbents on the superhydrophilic-nanostructured surface by an electrostatic coating method, which is a mature and effective coating technology with high material transfer efficiency to provide electrostatically bonded homogeneous monolayers on the surface [44]. The detailed procedures of these three steps follow.

2.1.1 Synthesis of the MWCNT-embedded zeolite 13X/$CaCl_2$ composite adsorbent

There are two main processes to synthesize the MWCNT-embedded zeolite 13X/$CaCl_2$ composite adsorbent [45], the first being the preparation of the zeolite 13X/$CaCl_2$ composite adsorbent and the second being MWCNT embedment. The $CaCl_2$ component can raise the adsorption capacity of the composite adsorbent in comparison with the pure zeolite 13X [46]. Embedding MWCNT into the adsorbent increases the thermal conductivity of the composite adsorbent, an important factor affecting the condensation heat transfer efficiency. The water vapor adsorption ability of the composite adsorbent is about 5 times larger than that of the pure zeolite 13X adsorbent. In addition, the effective thermal conductivity of the composite adsorbent utilized on the heterogeneous surfaces is 0.27 – 0.8 W/mK, while it is only 0.08 – 0.13 W/mK for the pure zeolite 13X, showing an improvement of 515% [45].

To synthesize the zeolite 13X/$CaCl_2$ composite adsorbent, the dried zeolite 13X powder (283595, Sigma-Aldrich) is mixed with 46 wt% of $CaCl_2$ solution with the mass ratio of 1:9. This step is for the ion exchange between the Ca^{2+} in the $CaCl_2$ solution and the Na^+ ions in zeolite 13X. The mixture is stirred by a magnetic stirrer for 24 hours and the excess $CaCl_2$ solution is filtered out. The residue on the filter paper is the zeolite 13X/$CaCl_2$ composite adsorbent which is then cleaned with deionized water. Afterwards, the composite adsorbent is removed carefully from the filter paper then dried in an oven at 150 °C for 24 hours to obtain its weight in the dry state. Afterwards, the dried composite adsorbent is mixed with the 40 wt% $CaCl_2$ solution with the mass ratio of the dried composite adsorbent to $CaCl_2$ at 1:1.5 to form the mixture. The MWCNT (TNM2, Timesnano) is added into the mixture with the mass ratio of the MWCNT to the mixture at 1:100. Next, the mixture is stirred with a magnetic stirrer for 24 hours and dried in the oven at 150 °C for 24 hours. After grinding into powder, the MWCNT-embedded zeolite 13X/$CaCl_2$ composite adsorbent is consequently fabricated.

2.1.2 Fabrication of the superhydrophilic-nanostructured surface

The second step is the fabrication of the superhydrophilic-nanostructured surface which is coated onto a copper substrate using a dip coating method [47]. In this study, square copper plates are used because copper has a relatively high thermal conductivity [48]. First, copper plates are prepared with the dimension of 45 mm × 45 mm × 3 mm (length × width × thickness) as the substrates. The copper substrates are then polished on one side with abrasive paper of 400, 600, 800, 1000, 1200, 1500, 2000 grits in sequence. After polishing, the surface of the

copper substrates is pinkish gold [49]. Residual grease on the samples is removed by soaking the copper plate in 100 ml acetone solution for 10 minutes. Next, the copper substrates are immersed into pure ethanol for another 10 minutes to remove the remaining acetone and are then rinsed by deionized water and blow-dried with nitrogen. Subsequently, the copper substrates are dipped into 100 ml 0.0115 M of silver nitrate solution ($AgNO_3$) for 18 minutes, causing the surface to gradually turn deep black as the nano-textured silver is deposited on the copper substrate surface [50]. After this step, the nano-coating is formed on the substrates. The substrates are then gently immersed in the deionized water bath and dried with nitrogen. To change the wettability of the nanostructured surface, the samples are then soaked in the 1 mM solution of 11-mercaptoundecan-1-undecano (MUD) in the dichloromethane (CH_2Cl_2) which is used as the wetting-surface agent [50] for 1 hour. Last, the substrates are immersed into pure ethanol for 1 minute, and then gently dried by nitrogen. Through the above procedures, the superhydrophilic-nanostructured surface is fabricated.

2.1.3 Electrostatic coating of the composite adsorbent on the superhydrophilic-nanostructured surface

The third step is to electrostatically coat the composite adsorbent on the superhydrophilic-nanostructured surface. The experimental intelligent electrostatic coating machine (COLO-800D-T-08C, HICOLO) is used in this study. The working voltage used for the electrostatic coating is 100 kV. The pressure of the input compressed air is 6 bar. First, the composite adsorbent powder is mixed with compressed air in a container in preparation to be sprayed on the superhydrophilic-nanostructured copper substrate. Before the spraying process, the composite adsorbent powder is charged using either a corona or a tribocharging gun [51]. A static field is generated when the electricity is connected, thus, charged adsorbent powder is sprayed to the grounded superhydrophilic-nanostructured surface with the help of air supplied to the gun. The composite adsorbent powder adheres to the superhydrophilic surface due to the electrostatic attraction force. A mass area ratio (MAR), which is defined as the ratio of the weight of the composite adsorbent coated on the surface to the area occupied by the adsorbent, is utilized to ensure a uniform coating thickness of the composite adsorbent on the superhydrophilic surfaces. The constant input working voltage and the pressure of the compressed air supply maintain the stable output rate of the composite adsorbent powder. In this study, the average spraying time used is 5 seconds for each sample. In order to make sure the samples are coated with a similar MAR of the composite adsorbent with a relative

difference less than 10% (15 ± 1.5 g/m^2), each sample is weighed before and after coating to obtain the weight of the composite adsorbent coated. With the same MAR of composite adsorbent coated on the surface, the thickness of the composite adsorbent can also be considered uniform. It should be noted that the composite adsorbent coating is robust and will not shed from the surface unless deliberately scratched. Customized acrylic covers are prepared by a laser cutter, which are placed over the superhydrophilic-nanostructured surface to form the different patterns of the composite adsorbents.

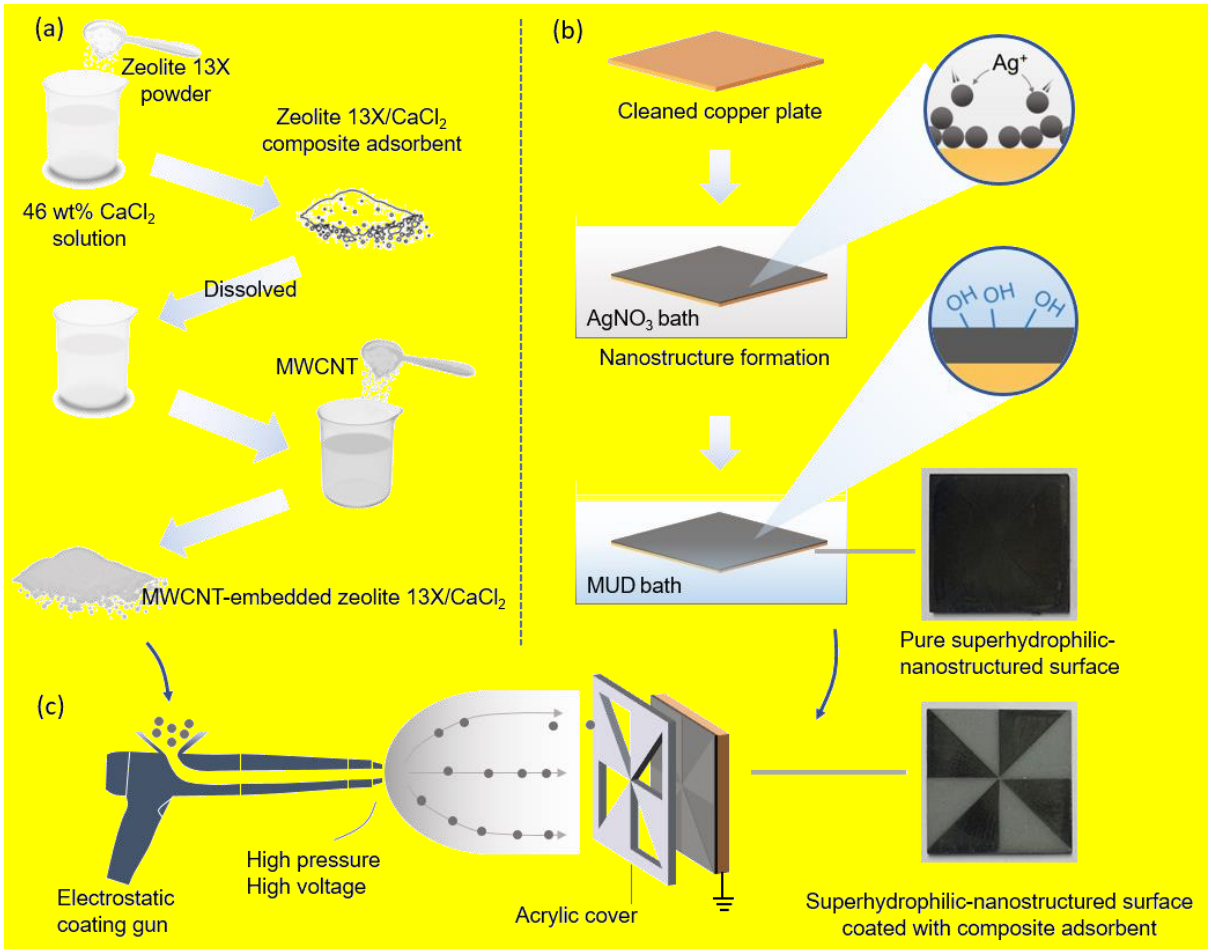

Figure 1. Fabrication process of the novel composite adsorbent coated superhydrophilic-nanostructured heterogeneous surface. (a) Fabrication process of MWCNT-embedded zeolite 13X/$CaCl_2$ composite adsorbent; (b) Fabrication process of the superhydrophilic-nanostructured surface; (c) Fabrication process of the heterogeneous surface via electrostatic coating.

With the three-step fabrication procedure described in Figure 1, different patterns of the novel heterogeneous surface are prepared. A total of 16 patterns are investigated in this study, which

are shown in Figure 2. The patterns are classified into 5 different groups. In particular, the reference group consists of the untreated copper plate, the pure superhydrophilic-nanostructured surface without the composite adsorbent coating, and the superhydrophilic-nanostructured surface completely covered with composite adsorbent. The middle stripe pattern group consists of the patterns with the middle composite adsorbent stripe consisting of different composite adsorbent area ratio (AAR), i.e., the ratio of the composite adsorbent area to the total area of the heterogeneous surface of 8.3%, 16.7%, 33.3%, 50%, 66.7% respectively. The AAR of the remaining groups (stripe group, triangular group and square group) are identical with 50% coverage of composite adsorbent.

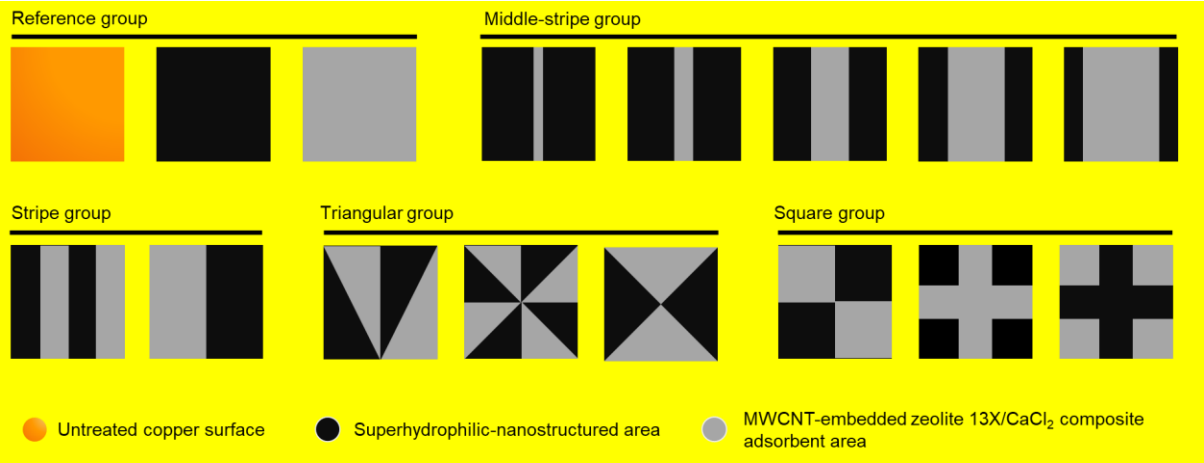

Figure 2. Different patterns designed and grouped. (Orange area is the untreated copper surface; Black area is the superhydrophilic-nanostructured surface; and Gray area represents the composite adsorbent covering)

2.2 Surface profile characterization

To verify that the heterogeneous surface is successfully fabricated, the contact angle measurement, optical surface profile measurement, and scanning electron microscope (SEM) are conducted. Figure 3(a) illustrates the wettability of the heterogeneous surface via the contact angle measurement. The static contact angle of the surfaces is measured by a contact angle meter (Biolin Theta, Attension) with an accuracy of ± 0.1°. 5 µL of deionized water droplets are placed at 5 different locations on the horizontal surfaces for measurement as shown in Figure 3(a). The results show that all of the static contact angles of the heterogeneous surfaces are less than 10° and the average contact angle is around 6.4°, demonstrating that the heterogeneous surfaces are superhydrophilic.

The profile of the heterogeneous surface and the thickness of the composite adsorbent coating are determined by an optical surface profiler (NT1100, Veeco Wyko) with an accuracy of ± 0.01 µm. The 3D surface profile measured by the optical surface profiler is shown in Figure 3(b). The thickness of the composite adsorbent sprayed on the surface is estimated by analyzing the 2D boundary data of the profile. The average composite adsorbent thickness is 23.00 ± 3.84 µm. In addition, SEM is also conducted to illustrate the crystal look-alike nano-grass structure of the superhydrophilic surface as shown in Figure 3(c). The SEM image of the composite adsorbent-coated area is shown in Figure 3(d). Our previous work [45] illustrated the total pore volume and pore size distribution of the MWCNT-embedded zeolite 13X/$CaCl_2$ composite adsorbent via the BET analysis, which shows the BET surface area of 8.83 m^2/g and the total pore volume of 0.053 cm^3/g. The pore size distributions are calculated through the Barrett-Joyner-Halenda (BJH) model, which is shown in Table 1. The overall specific surface area and total pore volume of the composite adsorbent increase due to the addition of MWCNT, which is beneficial for the faster diffusion of the water vapor into the inner pores of the composite adsorbent.

Table 1. Pore size distributions of the composite adsorbent via the BJH analysis [45]

Pore Diameter Range (nm)	**< 6**	**6-8**	**8-10**	**10-12**	**12-16**	**16-20**	**20-80**	**> 80**
Pore Volume (ml/g) $\times 10^2$	0.089	0.055	0.069	0.101	0.198	0.331	3.208	7.871
%	0.75	0.46	0.58	0.85	1.66	2.78	26.91	66.02

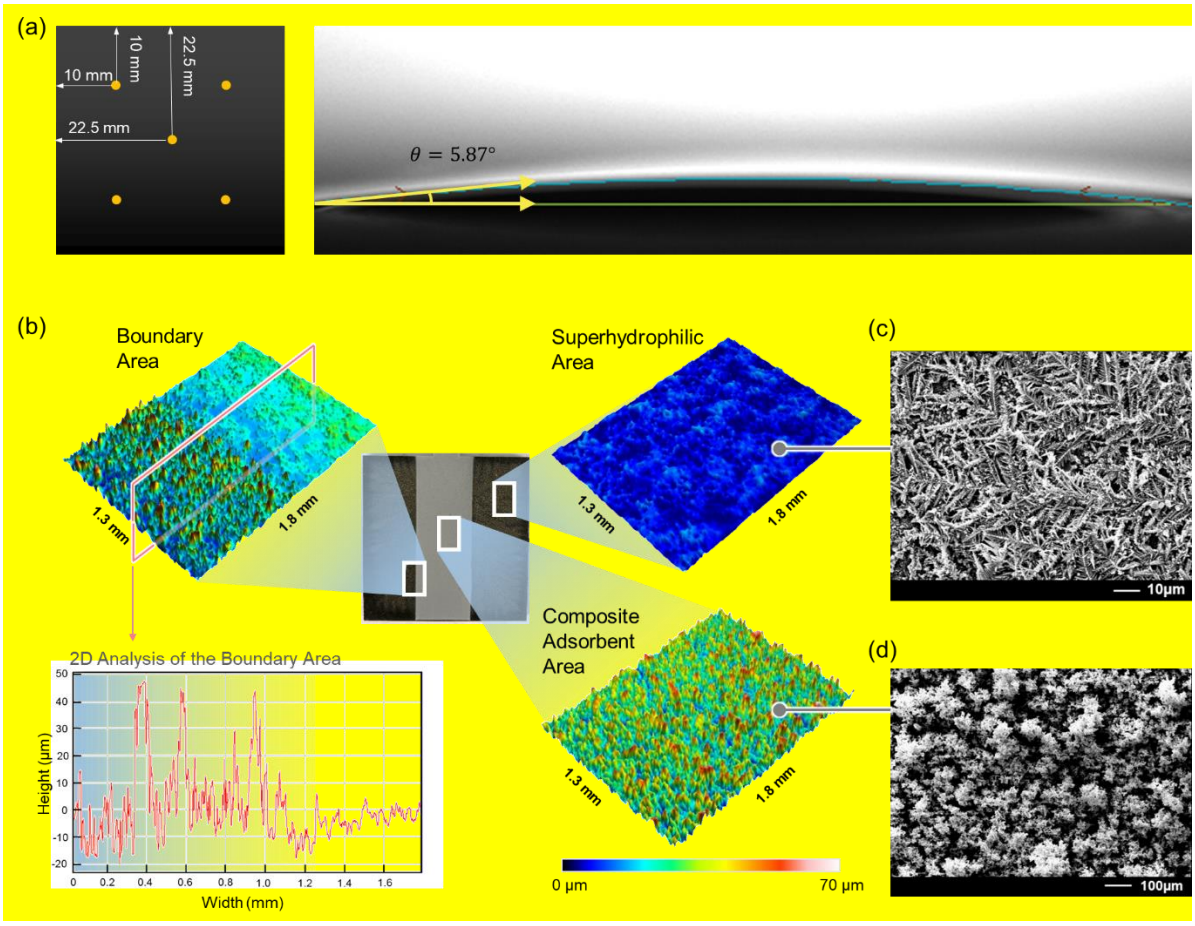

Figure 3. (a) Contact angle measurement of the pure superhydrophilic-nanostructured surface; (b) Surface morphology at different parts of the heterogeneous surfaces; (c) SEM image of the nanostructured-superhydrophilic surface; and (d) SEM image of the area coated with the composite adsorbent.

3 Methodology of Condensation Experiments

The condensation experiments are conducted to obtain the condensation rate of the surfaces. A schematic of the condensation experiments is shown in Figure 4(a). The copper heat exchanger with attached sample (heterogeneous surface) and water collection device are placed in a humidity-controlled acrylic chamber with a volume of 0.03 m^3. Dried airflow and a humid airflow are mixed before entering the chamber. By adjusting the two airflow valves, the relative humidity of the chamber can be controlled from 5% to 100%. The copper heat exchanger is connected with an isothermal refrigerated circulator (AP15R-30-A12E, Polyscience) with ± 0.01 °C uncertainty to maintain the constant temperature of the heat exchanger. A layer of thermally-conductive grease (707-4736, thermal conductivity = 5 W/mK, RS Pro) is applied between the sample and the copper heat exchanger to reduce thermal contact resistance. The heat exchanger is wrapped with a layer of thermal insulation sheet to avoid condensation

forming on the cold heat exchanger. The thickness of the thermal insulation layer is 5 mm. Since the isothermal refrigerated circulator has sufficient cooling power (915 W at 20 ºC) to provide the cooling effect, the substrate temperature (T_s) could be considered as constant, which is measured and recorded by a thermocouple (123-3218, RS Pro). The thermocouple is placed on the side of the sample at the bond point between the sample and the heat exchanger and is in contact with the thermally-conductive grease as shown in the insert figure of Figure 4a. Also, as shown in Figure S1 and Table S1 in Appendix A, the substrate temperature measurement has been verified via comparing the average substrate temperature with the measuring point, showing a small temperature deviation. During the experiment, the relative humidity (RH) and temperature of the air in the experimental chamber are real-time monitored by a temperature and relative humidity meter (982 probe, 7575-X-NB, TSI). The air inlet is set away from the location where the sample is placed during the condensation experiment and a windshield is fixed near the air inlet to slow down the air flow. An airflow velocity meter (964 probe, 9565-P-NB, TSI) is used to measure the air velocity inside the chamber while maintaining the experimental condition of RH = 95%, as the curve shows in Figure S2 of Appendix A, and an average air velocity of 0.005 m/s is obtained, which is negligible. In this case, the experimental environment in the chamber can be considered as a steady, nearly windless environment. The experiments are conducted under the atmospheric pressure condition and the condensing fluid is the water vapor from air. The condensed water that shed from the sample over a specific time period is weighed by a weight balance (KB 1000-2, KERN) with 1-minute interval. A photo of the condensation experiment setup is shown in Figure 4(b). For each sample, the condensation experiments are repeated four times under the same conditions. Data collection starts when the experimental condition stabilizes. The final value of the water condensation rate, $\dot{m}_w$, for each sample is obtained by averaging the values.

The uncertainties of the water condensation experiments are associated with the temperature and air humidity meter (i.e. ± 3%), the cooling power of the isothermal water circulator (i.e. ± 1%), the weight balance which includes the time interval for data collected (i.e. ± 3.3%) and the measurement of dimensions (i.e. ± 5%). The uncertainties caused by moisture evaporation (i.e. ± 4.4% to 9.2%) during the water collection process are estimated by conducting a control experiment, where the weight of the water in a beaker is continuously recorded under the relative humidity of 95%. The overall uncertainty $\delta_{\dot{m}_w}$ of the water condensation rate is mainly

related to the weight of the water collected over time and the effective heat transfer area that contribute to $\dot{m}_w$, while $\delta_{\dot{m}_w}$ can be estimated by the following equation:

$$\delta_{\dot{m}_w} = \pm\sqrt{{\delta_W}^2 + {\delta_A}^2 + {\delta_E}^2} \quad , \tag{1}$$

where δ_W, δ_A, δ_E are the uncertainties of the weight balance, the effective heat transfer area and the water evaporation, respectively. $\delta_{\dot{m}_w}$ is estimated as ±8.1% ~ ± 11.4% according to Eq. (1).

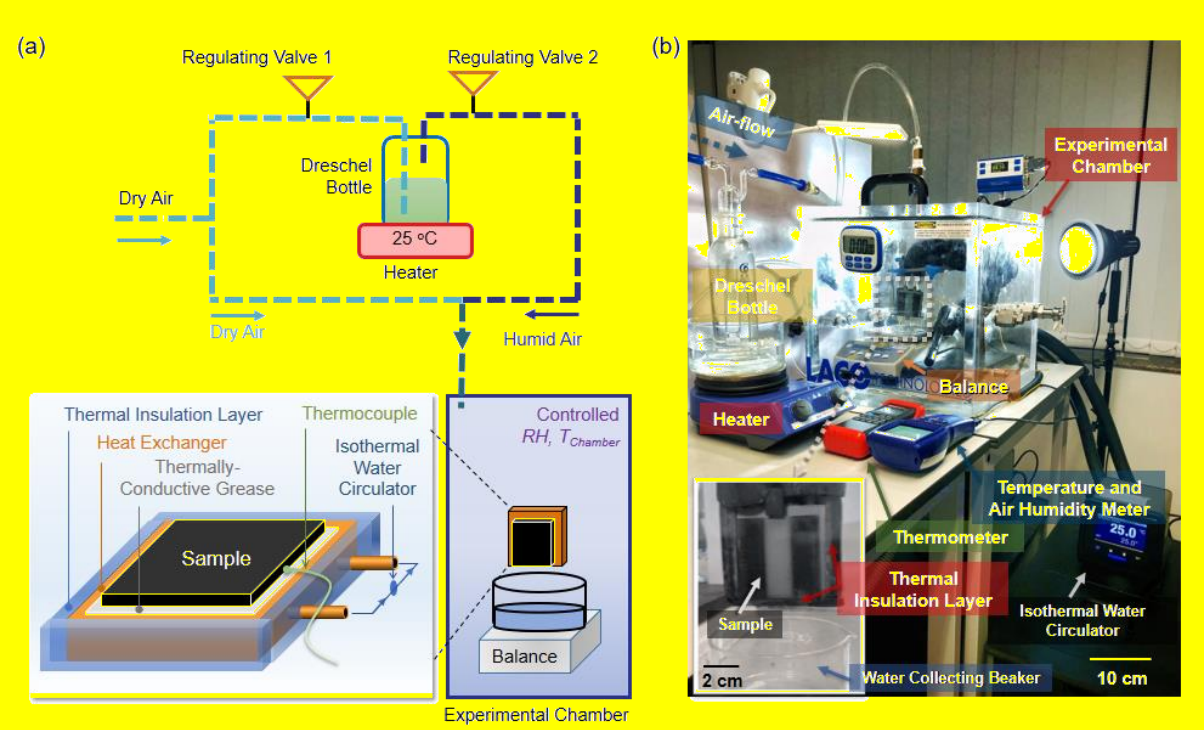

Figure 4. (a) Schematic and (b) photo of the condensation experiment

The overall heat transfer on a surface with the existence of non-condensable gas (NCG) includes latent heat transfer and sensible heat transfer. In this study, the average substrate temperatures during the condensation experiments are set as 8 °C, 11 °C, and 14 °C. This corresponds to the temperature difference between the ambient temperature and the substrate temperatures ($T_\infty - T_s$) values of 15 °C , 12 °C , and 9 °C , respectively. With considering forced convection over the 4.5 cm × 4.5 cm vertical plate and an average air flow velocity of 0.005 m/s (according to the results shown in S2 of Appendix A), the sensible heat flux can be estimated as 1.313 $W/m^2 \cdot K$, 1.313 $W/m^2 \cdot K$, and 1.314 $W/m^2 \cdot K$ corresponding to the

substrate temperatures of 8 °C, 11 °C, and 14 °C, respectively. The substrate temperature of the samples can be considered as constant since the isothermal water circulator provides sufficient cooling power to the surface. Therefore, for different samples under the same experiment condition, the sensible heat transfer between the surface and the ambient is assumed to be the same [31, 52]. Considering the sensible heat flux value is relatively small due to the nearly windless experimental setting, the contribution from the sensible heat flux for different patterned heterogeneous surfaces under the identical experimental condition would remain the same. In this case, differences in the condensation heat transfer performance among the different heterogeneous surfaces are mainly reflected by the latent heat transfer component. In order to evaluate the latent heat part of the heat transfer of the heterogeneous surfaces, the latent heat transfer (LHT) coefficient (C_{LTH}) is specifically calculated and can be determined by [53]

$$C_{LTH} = \frac{\dot{m}_w h_{fg}}{T_{dew} - T_s}, \quad (2)$$

where $\dot{m}_w$ is the water condensation rate, h_{fg} is the latent heat of condensation, T_{dew} is the dew point temperature and T_s is the substrate temperature. The water condensation rate, $\dot{m}_w$, is obtained from the condensation experiments. C_{LTH} is defined as the heat transferred per unit area per kelvin due to the state change of the water vapour. The heat flux from condensation of the water vapour from air is the main contributor of the latent heat transfer in this study. According to Eq. (2), the water condensation performance of different samples results in different values of C_{LTH}. The uncertainties of the latent heat transfer coefficient are estimated by the following equation:

$$\delta_C = \pm\sqrt{\left(\frac{\partial C}{\partial \dot{m}_w}\right)^2 \cdot (\delta_{\dot{m}_w})^2 + \left(\frac{\partial C}{\partial T_s}\right)^2 \cdot (\delta_{T_S})^2}\ , \quad (3)$$

where δ_C, $\delta_{\dot{m}_w}$, δ_{T_S} are the uncertainties of the latent heat transfer coefficient, the condensation rate and the substrate temperature difference, respectively. δ_C is estimated as ± 1.3% ~ ± 7.0% according to Eq. (3).

Besides, as the C_{LTH} is closely related to T_{dew} and T_s, the effects of dew point temperature and substrate temperature on the condensation heat transfer performance are also investigated [54]. The dew point temperature in the condensation experiments is controlled by adjusting the air

humidity while keeping the same dry bulb temperature. Different environmental parameters and different substrate temperatures used in the condensation experiments are shown in Table 2. The ambient temperature and the relative humidity are chosen according to the local weather conditions in Hong Kong [55]. In addition, the influence of substrate sub-cooling on latent heat transfer performance is investigated with different substrate temperatures under the chosen air conditions.

Table 2. Parameters in the condensation experiment

Parameters	**Values**	**Unit**
Pressure	1.05×10^5	Pa
Ambient Temperature	23 ± 2	°C
Relative Humidity	55, 75, 95	%
Corresponding Dew Point	13.5, 18.3, 22.1	°C
Substrate Temperature	8, 11, 14	°C
Corresponding Latent Heat of Condensation	2482.5, 2475.4, 2468.3	kJ/kg

4. Results and Discussion

4.1 Distributions of the latent heat transfer coefficient under different dew point temperatures and substrate temperatures

The box plot is utilized to present the overall results distributions of the 16 samples under different conditions. As shown in Figure 5, box plots present the maximum, minimum, average, median, lower and upper quartiles of the C_{LTH} of all the surfaces, including the plain copper surface, the pure superhydrophilic-nanostructured surface, and the patterned composite adsorbent coated superhydrophilic-nanostructured surface, at different dew point temperatures (substrate temperature is identical (8 °C)) [Figure 5(a)] and different substrate temperatures (dew point temperature is identical (22.1 °C)) [Figure 5(b)]. The deviations and statistical distributions of the data set are easily reflected by the box plot, where large deviations indicate the larger latent heat transfer performance difference under a specific condition. It can be seen that the average C_{LTH} increases as the dew point temperature increases, which is due to high water content in the air under the same ambient temperature. Besides, it can be also observed that under a higher dew point temperature or lower substrate temperature, the deviations of C_{LTH} are also larger since the difference between the dew point temperature and the substrate temperature is the driving force for the net water vapor flux toward the substrate, and larger

differences may affect the condensation performance more significantly. With larger deviations of the dataset, the differences of latent heat transfer coefficient among different surfaces could be obviously observed. Therefore, the experimental condition, i.e., high dew point temperature (22.1 ºC) and low substrate temperature (8 ºC), is chosen to further analyze the impact of different composite adsorbent patterns on the condensation heat transfer performance.

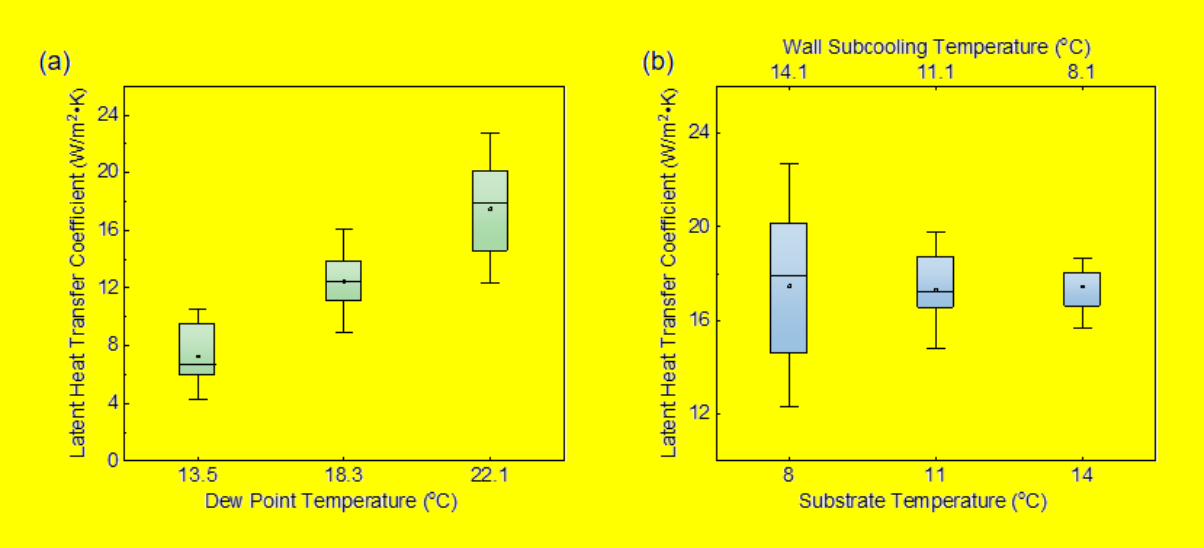

Figure 5. (a) Box plot of the condensation experimental results of all the samples under different dew point temperatures (i.e., 13.5 ºC, 18.3 ºC, 22.1 ºC) at the substrate temperature of 8 °C; and (b) Box plot of the condensation experimental results of all the samples under different substrate temperatures (i.e., 8 °C, 11 °C, 14 °C) at the dew point temperature of 22.1 ºC.

4.2 Comparison of the condensation rate of different heterogeneous surfaces

Figure 6 shows the amount of the water collected per unit area of the sample against time under the condition of 22.1 ºC dew point temperature and 8 ºC substrate temperature. The increment rate of the water collected tends to stabilize over time and the determination coefficients, R^2, of the three fitting curves are all over 0.99, thus it is believed that the rate of the water collected remains unchanged when the experiment is conducted for a longer time, i.e., the condensation experiment reaches the steady state. In this way, the slopes of the lines calculated can be used as the condensation rate, $\dot{m}_w$ ($g/min \cdot m^2$), accurately, which are 7.44 $g/min \cdot m^2$, 5.92 $g/min \cdot m^2$, and 4.30 $g/min \cdot m^2$ for the superhydrophilic-nanostructured surface fully covered with the composite adsorbent, pure superhydrophilic-nanostructured surface, and pure

copper plate, respectively. Among the three surfaces, the superhydrophilic-nanostructured surface fully covered with the composite adsorbent shows the best water condensation rate. This is because when the superhydrophilic-nanostructured surface is coated with the composite adsorbent, the porous composite adsorbent has a positive effect on condensation heat transfer by adsorbing the water vapor from the ambient air due to its physical (porous structure) and chemical ($CaCl_2$) adsorption ability.

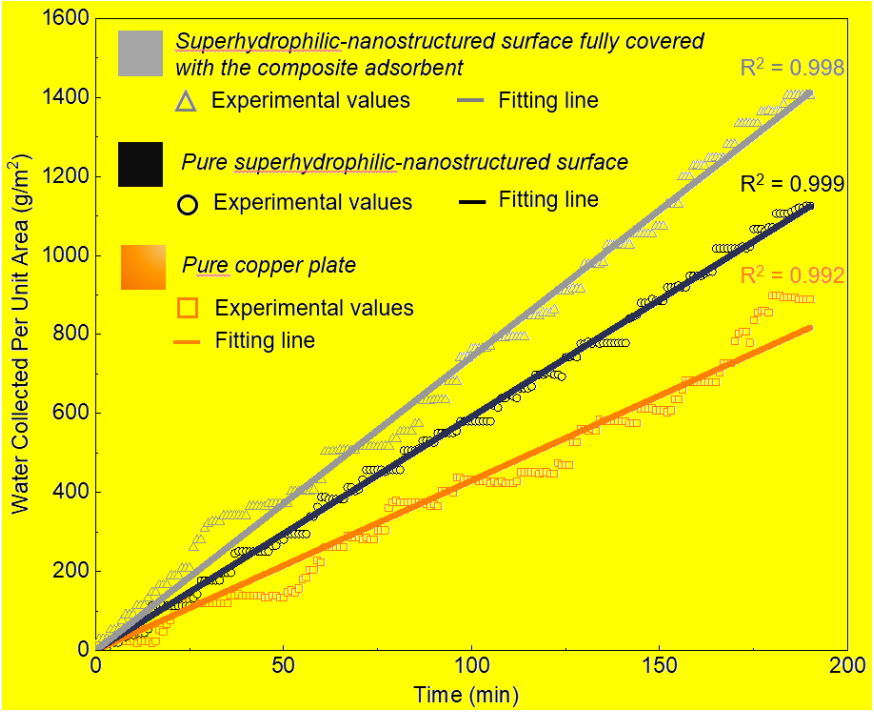

Figure 6. Cumulative water collection mass (g/m^2) against time (min) of the superhydrophilic-nanostructured surface fully covered with the composite adsorbent, pure superhydrophilic-nanostructured surface and pure copper plate under the condition of $T_{dew} = 22.1\ ^0C$ and $T_s = 8\ ^0C$.

4.3 Comparison of the latent heat transfer coefficient with different composite adsorbent patterns

The composite adsorbent coated superhydrophilic-nanostructured heterogeneous surfaces are grouped according to the pattern shapes, i.e., stripe, square and triangle. The comparison of the average C_{LHT} of three groups is shown in Figure 7(a), where the average C_{LHT} is defined as the mean value among the patterns in each group as shown in Figure 7(a). In addition, the C_{LHT} of the patterns with the AAR of 50% in each shape group are also illustrated in Figure 7(a). Comparing the average C_{LHT} in each group, it is found that the patterns with the vertical stripe

shape have a better condensation heat transfer performance than the patterns with square and triangle shapes. This can be attributed to the fast condensate transport characteristic (i.e. water removal from the surface) of the superhydrophilic-nanostructured surface, which has been suggested by previous research that superhydrophilic regions in the parallel-striped hydrophilic-superhydrophilic surfaces can provide a path for condensed water drainage [52]. In addition, water film adsorption mechanism, namely the water-free region that appears in the superhydrophilic region adjacent to the composite adsorbent, is observed due to the high water adsorption ability of the composite adsorbent. The superhydrophilic region whose water film is adsorbed by the composite adsorbent provides new nucleation sites, improving the condensation rate, and hence enhancing the condensation heat transfer of the surface. The detail of this phenomenon will be further discussed in the following section.

Besides, the C_{LHT} of different stripe shaped patterns in different orientations (i.e. vertical and horizontal) are also studied and compared. The results in Figure 7(b) show that the horizontal stripe adsorbent patterns have smaller C_{LHT} than that of the vertical stripe patterns. This can be explained by the different water removal rates of patterns with stripe shapes in different orientations. It should be noted that the water removal rate plays a critical role for condensation heat transfer enhancement since the water film on the surface leads to increased thermal resistance (i.e., between the surface and ambient air) that causes a large decline in the heat transfer efficiency. In addition, the removal of the condensed water is gravity induced. Thus, the composite adsorbent patterns with vertical stripes that are parallel to gravity offer more efficient water drainage channels than horizontal stripes. Overall, the orientations of the composite adsorbent patterns play an important role for the condensation heat transfer performance.

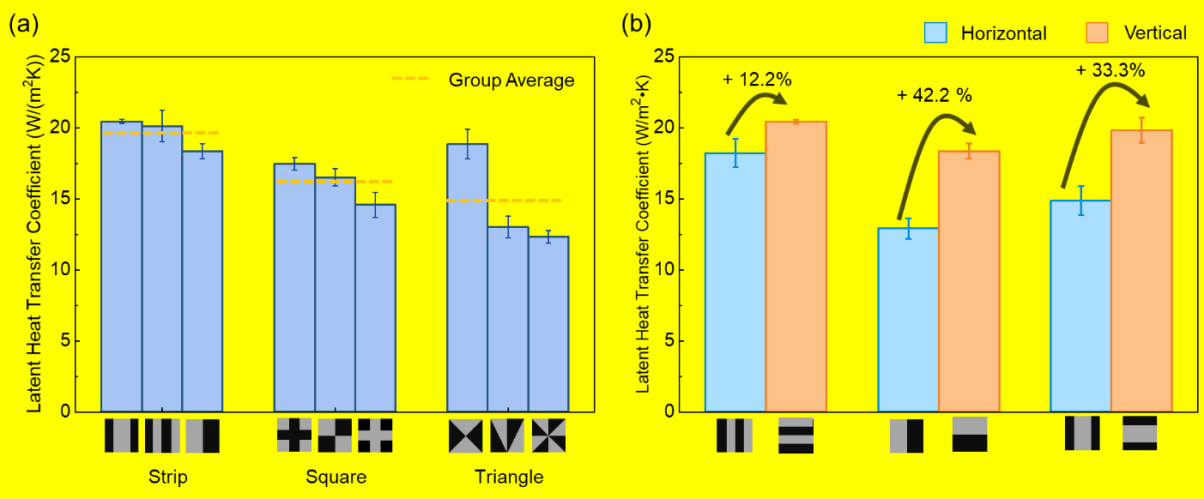

Figure 7. (a) C_{LHT} comparison of the composite adsorbent patterns with different shapes (i.e. stripe, square and triangle) and the rank of the C_{LHT} of the patterns with similar shape (i.e. water condensation rate in each sub-group decreases from left to right); and (b) C_{LHT} comparison of the composite adsorbent patterns with stripe shapes in different orientations (i.e. vertical and horizontal)

4.4 Comparison of the latent heat transfer coefficient of the vertical stripe patterns with different composite adsorbent area ratios (AARs)

As the heterogeneous surfaces with vertical stripe patterns are found to have relatively higher condensation heat transfer performance than others, the effects of the AAR of the vertical-striped composite adsorbent pattern on the condensation heat transfer performance are further studied. The experimental results of vertical-striped composite adsorbent patterns with different AARs under the same experimental conditions ($T_{dew} = 22.1$ ℃ and $T_s = 8$ ℃) are shown in Figure 8(a). Compared with the plain copper plate and pure superhydrophilic-nanostructured surface, the heterogeneous surface with the vertical stripes pattern (i.e., AAR = 33.3%, 15 mm wide) can improve the C_{LHT} by 80.0% and 30.8%, respectively. It can also be seen that when the AAR is less than one-third, the C_{LHT} increases with the increase of AAR. After reaching the maximal value, when the AAR equals one-third, the C_{LHT} decreases with the increase of AAR. The trend of the C_{LHT} variation with the increase of the AAR is associated with the water film adsorption mechanism, which will be further investigated below in a detailed manner.

As mentioned previously, the water film adsorption mechanism in the superhydrophilic region adjacent to the coated composite adsorbent is observed. Specifically, during the condensation

experiments on the superhydrophilic surfaces with the vertical stripe patterns of the composite adsorbent, a water-free region forms at the interface between the composite adsorbent and the superhydrophilic surface, as shown in Figure 8(b). The water-free region is a gap without water film, which is formed due to high water adsorption ability of the composite adsorbent. Most importantly, the wettability of the gap region is superhydrophilic, which can provide clear nucleation sites for condensation due to its high surface energy. Therefore, new condensed droplets continuously form on this water-free region. In this way, the condensation process is accelerated by the water film adsorption mechanism, which is mainly attributed to the strong condensed water adsorption ability of the coated composite adsorbent and the nucleation sites renewed on the superhydrophilic region.

To verify the water film adsorption mechanism, a simple water adsorption test is conducted, as shown in Figure 8(c). In order to clearly demonstrate that the composite adsorbent can adsorb water film from the superhydrophilic surface, a bare copper gap (1.8 mm wide) is deliberately made at the junction between the composite adsorbent and the superhydrophilic surface. The intermediate bare copper area on the heterogeneous surface neither belongs to the superhydrophilic surface nor to the composite adsorbent coated surface, therefore, it is relatively fair for both surfaces to adsorb the water. It can be seen from Figure 8(c) that when a water droplet drops on the bare copper area, it diffuses faster on the composite adsorbent region than the superhydrophilic area. The dynamic process of the water film adsorption mechanism on the heterogeneous surface can also be seen in the video in Appendix B. At t = 1 s and t = 5 s, the water on the composite adsorbent and the superhydrophilic surface is connected, while at t = 10 s, the water connection is broken. By comparing the status of the surfaces at t = 1 s and t = 5 s, it can be further observed that when the water is connected, the composite adsorbent is able to adsorb the water from the superhydrophilic surface since the wetted area on the superhydrophilic surface keeps shrinking from t = 1 s to t = 5 s. After t = 10 s, when the water connection is broken, the composite adsorbent is unable to adsorb the water from the superhydrophilic surface such that the water on the superhydrophilic area begins to diffuse. The water adsorption test proves that the water adsorption ability would be improved with the addition of composite adsorbent. The strong water suction ability of the composite adsorbent results from the existence of the nano-scaled pores, which contribute to an increase in surface energy. Porous structures physically adhere on the superhydrophilic-nanostructured surface to form an overlapping surface area, which increase the roughness and the wicking

capability of the surface and further improve the surface energy. Compared with the pure superhydrophilic area, the area with the composite adsorbent overlapped shows a larger surface tension, therefore attracting the water molecules into its area. With the extra effect of the horizontal capillary force in the porous composite adsorbent, the composite adsorbent coated area is able to adsorb water from the superhydrophilic surface. During the condensation experiments, the samples would be placed vertically. The vertical capillary force of the composite adsorbent may cause resistance as the condensed liquid falls. A Bond number (Bo) is utilized to compare the effects of gravity and capillary forces [56]. Bo is ratio of the gravitational force to capillary forces, which is given by the equation:

$$\mathrm{Bo} = \frac{\Delta\rho g L^2}{\gamma}, \quad (4)$$

where $\Delta\rho$ is the density difference between the fluids, g is the acceleration of gravity, γ is liquid-gas surface tension, and L is a characteristic length. A low Bo value (Bo < 1) indicates capillary forces dominate. In contrast, a high Bo value (Bo > 1) indicates that gravity dominates and the system is relatively unaffected by the capillary force. In this study, the water-air system with the radius of the water droplet as the characteristic length is considered. The relationship between the radius of the water droplet and the Bo number is shown in Figure S3 of the Appendix A. When the water starts to condense, the droplet would go through a period when the capillary forces of the surface dominate. After the droplet grows to the size over 2.76 mm radius, the gravity starts to dominate, thus the droplet can drop from the surface. The average radius of the droplet dropped from the surface during the condensation experiment is 3.50 mm (Bo = 1.61) where the gravity dominates. During the experiments, water film condensed on the superhydrophilic surface can be adsorbed by the adjacent composite adsorbent and the adsorbent coated area could gather the condensed water quickly to overcome the capillary force of the composite adsorbent.

During the condensation experiments, the water film condensed on the superhydrophilic surface can be adsorbed by the adjacent composite adsorbent to form a water-free region, therefore enhancing the surface heat transfer performance. This is determined as the water film adsorption mechanism in this study. The mechanism of the heat transfer enhancement of the heterogeneous surface and the water film adsorption mechanism is further illustrated with the schematic shown in Figure 8(d). The condensed water forms a liquid film on the substrate

because the wettability is superhydrophilic, most of the liquid near the interface is drawn from the superhydrophilic-nanostructured surface to the composite adsorbent owing to its high water adsorption ability, while a small fraction of the condensed water diffuses towards the other side due to the water molecular cohesion and the high solid surface adhesion of the superhydrophilic-nanostructured surface [57] (State A). Therefore, a gap without water film (the water-free region) appears at the superhydrophilic region near the interface between the composite adsorbent and the superhydrophilic surface (State B). Since the superhydrophilic-nanostructured surface without water film can enhance water vapor nucleation sites, new nucleation could be formed on the water-free region (State C). It should be noted that State C is of short duration since the water droplet will become a water film due to the high surface energy of the superhydrophilic surface. In this way, State C will turn back to State A, forming a cycle. According to the condensation experimental results of the composite adsorbent coated heterogeneous surface with AAR of 33.3% as shown in Figure S4 in Appendix A, a constant condensation rate of the composite adsorbent coated heterogeneous surface is observed regardless of water adsorption capacity of the adsorbent, meaning that water adsorption performs much faster than water vapour nucleation and the water-free region always exists during the condensation process. Therefore, State A is also an instantaneous state. The water-free regions with the surface wettability of superhydrophilic could serve as favorable nucleation sites to improve the condensation heat transfer performance because of the substantially minor interfacial energy barrier between superhydrophilic region and the water vapor [33]. Consequently, the condensation heat transfer performance of the heterogeneous surfaces could be enhanced by the water film adsorption mechanism. This water film adsorption mechanism on the heterogeneous surface also functions to accelerate the water removal, which is similar to the patterned hydrophilic-hydrophobic composite surfaces [28, 29, 33, 34], where fresh nucleation sites are effectively renewed, improving the condensation heat transfer performance [29]. Also, with the addition of the highly thermal conductive nanomaterial, MWCNT, the effective thermal conductivity of the composite adsorbent layer could be enhanced, which helps achieve a better surface heat transfer performance [28]. Simultaneously, the water-free region always exists on the heterogeneous surface during the condensation process, meaning that no extra time and energy are required to regenerate the composite adsorbent on the heterogeneous surface to maintain its condensation performance.

As discussed above, the C_{LHT} in Figure 8(a) first presents an increasing trend then a decreasing trend with the increase of AAR. This phenomenon may be the result of the trade-off effects provided by area ratio of the composite adsorbent region and the superhydrophilic region. The effect of the water film absorption mechanism would increase as AAR increases since more composite adsorbent increases the adsorption capability. However, the area for nucleation (i.e., superhydrophilic area) becomes insufficient with a larger AAR. Therefore, even when the water film adsorption mechanism has a positive effect on condensation heat transfer with the increase of AAR, the increasing trend of the C_{LHT} moderates due to the decrease in area for nucleation. Due to the composite adsorbent, larger AAR may lead to an increase in thermal resistance of the surfaces, which may be responsible for the decreasing trend since the negative effect on the latent heat transfer offsets the positive effect from the increment of AAR. With interactions between the positive effect provided by the water film adsorption mechanism and the negative effect provided by the thermal resistance, the trade-off effect of different AARs could be observed. This could explain why there exists an optimal point of the C_{LHT} value when the AAR is increased.

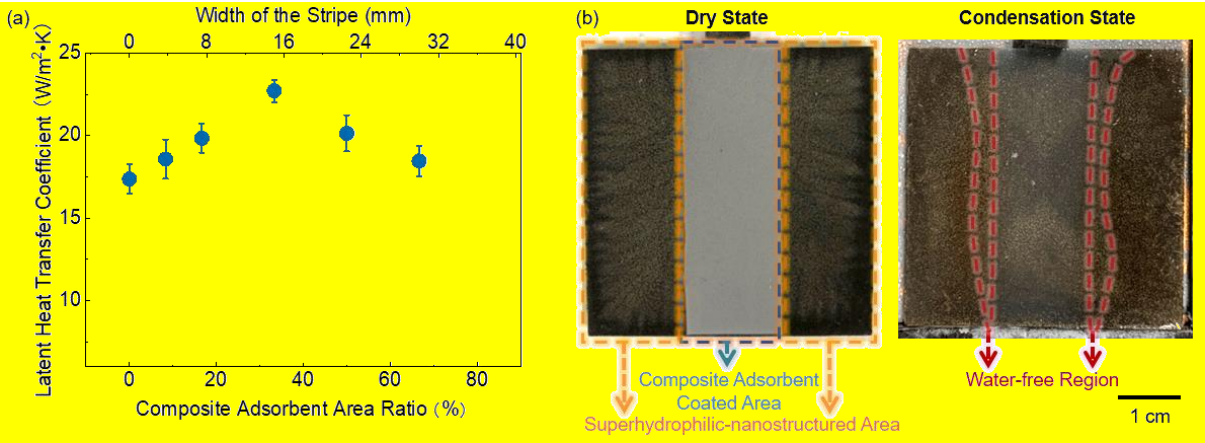

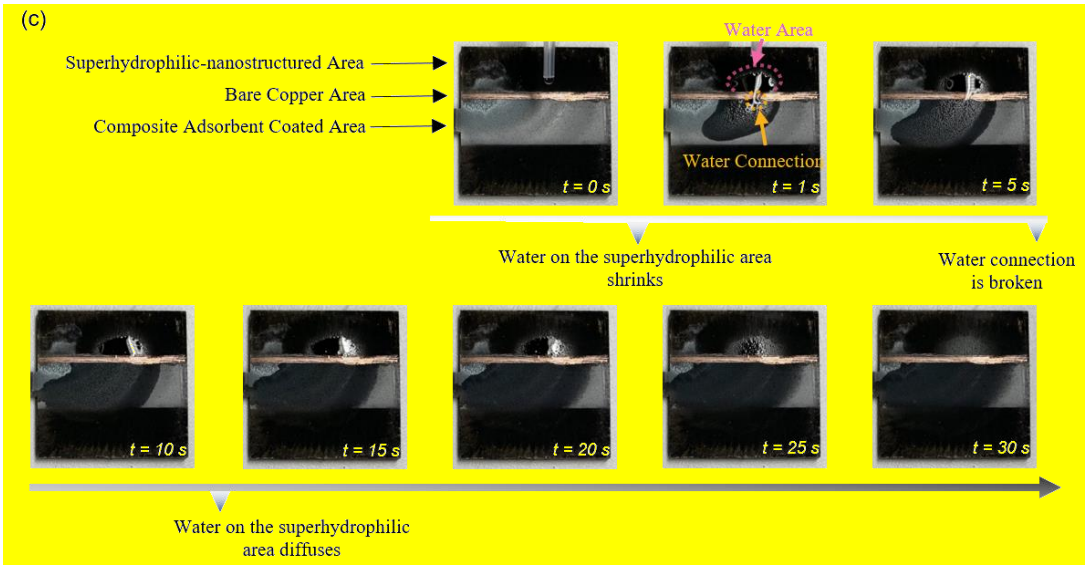

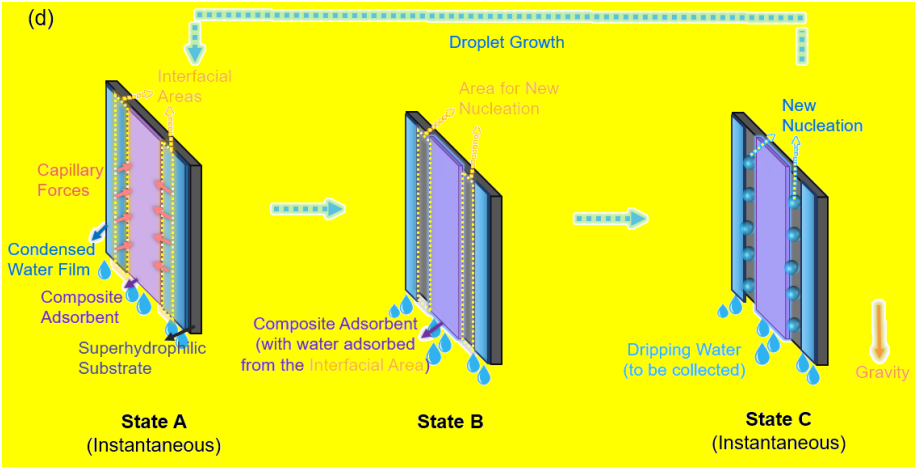

Figure 8. (a) The C_{LHT} of the heterogeneous surfaces with the vertical stripe composite adsorbent patterns against different AARs and widths of the stripe; (b) Photos of the water film adsorption mechanism (condensation state) on the heterogeneous surface; (c) Water diffusion behavior on the heterogeneous surfaces; and (d) Schematic of water film adsorption phenomenon on the heterogeneous surface.

5. Conclusion

In this work, a novel composite adsorbent coated superhydrophilic-nanostructured heterogeneous surface with different patterns is proposed for the efficient filmwise condensation heat transfer enhancement. The condensation heat transfer coefficient of different heterogeneous surfaces is studied experimentally, and the results are compared with a plain copper plate and a pure superhydrophilic-nanostructured surface. The influences of the dew point temperature and substrate temperature on the condensation rate of different

heterogeneous surfaces are also investigated. It is found that at a lower substrate temperature or higher dew point temperature, the variations of the condensation rate of the heterogeneous surface are more significant. For various composite adsorbent patterned heterogeneous surfaces, the vertical stripe is found to have the best condensation heat transfer performance due to the fast water removal rate, showing 45.5% to 80.0% improvement compared to the copper surface. In addition, the C_{LHT} variations of the vertical stripe composite adsorbent coated patterns with different AARs are also investigated. The trend of C_{LHT} shows the optimal AAR is one third, which can be explained by the water film adsorption mechanism on the heterogeneous surfaces, another new finding of this work. In the future, it is highly recommended that more comprehensive studies should be conducted so that the water film adsorption mechanism can be fully utilized to enhance the condensation heat transfer. Last, it is worth noting that this heterogeneous surface, which can be easily fabricated in a large scale, has the potential to be used in many thermal-related applications, such as air-conditioning systems, dehumidifiers, passive radiative coolers, and adsorption cooling systems to further improve the condensation heat transfer performance.

CRediT authorship contribution statement

Siru Chen: Conceptualization, Methodology, Formal analysis, Investigation, Writing - original draft, Visualization. **Aiqiang Pan:** Methodology, Formal analysis, Writing - original draft. **Yihao Zhu:** Data curation, Visualization, Writing - review & editing. **Tsz Chung Ho:** Methodology, Investigation, Writing - review & editing. **Hau Him Lee:** Investigation, Validation, Writing - review & editing. **Yijun Zeng:** Methodology, Investigation, Writing - review & editing. **Chili Wu:** Validation, Writing - review & editing. **Hui He Qiu:** Resource, Writing - review & editing. **Chi Yan Tso:** Conceptualization, Methodology, Resource, Supervision, Writing - review & editing, Project administration, Funding acquisition.

Acknowledgments

The funding for this research is provided by the Hong Kong Research Grant Council (RGC) via Early Career Scheme (ECS) account 21200819, and Innovation and Technology Commission via Innovation and Technology Fund (ITF) account ITS/429/18 as well as City University of Hong Kong Internal Fund via the account of 9678165.

Declaration of Competing Interest

The authors declare that they have no known competing financial interests or personal relationships that could have appeared to influence the work reported in this paper.

References

[1] M.W. Browne, P.K. Bansal, An overview of condensation heat transfer on horizontal tube bundles, Applied Thermal Engineering, 19(6) (1999) 565-594.
[2] A. Magrini, L. Cattani, M. Cartesegna, L. Magnani, Integrated systems for air conditioning and production of drinking water–Preliminary considerations, Energy Procedia, 75 (2015) 1659-1665.
[3] A. Lee, M.-W. Moon, H. Lim, W.-D. Kim, H.-Y. Kim, Water harvest via dewing, Langmuir, 28(27) (2012) 10183-10191.
[4] O. Ozkan, E.D. Wikramanayake, V. Bahadur, Modeling humid air condensation in waste natural gas-powered atmospheric water harvesting systems, Applied Thermal Engineering, 118 (2017) 224-232.
[5] D.M. Warsinger, K.H. Mistry, K.G. Nayar, H.W. Chung, J.H. Lienhard, Entropy generation of desalination powered by variable temperature waste heat, Entropy, 17(11) (2015) 7530-7566.
[6] S. Sideman, D. Moalem, R. Semiat, Performance improvement of horizontal evaporator-condenser desalination units, Desalination, 21(2) (1977) 221-233.
[7] J. Campen, G. Bot, SE—Structures and Environment: Dehumidification in Greenhouses by Condensation on Finned Pipes, Biosystems Engineering, 82(2) (2002) 177-185.
[8] N. Miljkovic, E.N. Wang, Modeling and optimization of hybrid solar thermoelectric systems with thermosyphons, Solar Energy, 85(11) (2011) 2843-2855.
[9] T. Huhtamäki, X. Tian, J.T. Korhonen, R.H. Ras, Surface-wetting characterization using contact-angle measurements, Nature Protocols, 13(7) (2018) 1521-1538.
[10] A. Leipertz, A.P. Fröba, Improvement of condensation heat transfer by surface modifications, Heat transfer engineering, 29(4) (2008) 343-356.
[11] X. Hu, Q. Yi, X. Kong, J. Wang, A Review of Research on Dropwise Condensation Heat Transfer, Applied Sciences, 11(4) (2021) 1553.
[12] R. Erb, E. Thelen, Promoting permanent dropwise condensation, Industrial & Engineering Chemistry, 57(10) (1965) 49-52.
[13] Z. Qi, Z. Dongchang, L. Jifang, Surface materials with dropwise condensation made by ion implantation technology, International Journal of Heat and Mass Transfer, 34(11) (1991) 2833-2835.
[14] Q. Zhao, B. Burnside, Dropwise condensation of steam on ion implanted condenser surfaces, Heat Recovery Systems and CHP, 14(5) (1994) 525-534.
[15] A. Das, H. Kilty, P. Marto, G. Andeen, A. Kumar, The use of an organic self-assembled monolayer coating to promote dropwise condensation of steam on horizontal tubes, J. Heat Transfer, 122(2) (2000) 278-286.
[16] X. Luo, M. Wei, M. Cao, Preparation of superhydrophobic Cu mesh with corrosion resistance and applications in oil-water separation, Journal of Materials Engineering, 46(5) (2018) 92-98.
[17] W. Geng, A. Hu, M. Li, Super-hydrophilicity to super-hydrophobicity transition of a surface with Ni micro–nano cones array, Applied Surface Science, 263 (2012) 821-824.
[18] G. He, K. Wang, The super hydrophobicity of ZnO nanorods fabricated by electrochemical deposition method, Applied Surface Science, 257(15) (2011) 6590-6594.

[19] N. Miljkovic, R. Enright, Y. Nam, K. Lopez, N. Dou, J. Sack, E.N. Wang, Jumping-droplet-enhanced condensation on scalable superhydrophobic nanostructured surfaces, Nano Letters, 13(1) (2013) 179-187.
[20] G. Azimi, R. Dhiman, H.-M. Kwon, A.T. Paxson, K.K. Varanasi, Hydrophobicity of rare-earth oxide ceramics, Nature Materials, 12(4) (2013) 315-320.
[21] R.N. Wenzel, Resistance of solid surfaces to wetting by water, Industrial & Engineering Chemistry, 28(8) (1936) 988-994.
[22] A. Cassie, S. Baxter, Wettability of porous surfaces, Transactions of the Faraday Society, 40 (1944) 546-551.
[23] N. Miljkovic, R. Enright, E.N. Wang, Effect of droplet morphology on growth dynamics and heat transfer during condensation on superhydrophobic nanostructured surfaces, ACS Nano, 6(2) (2012) 1776-1785.
[24] M.M. Derby, A. Chatterjee, Y. Peles, M.K. Jensen, Flow condensation heat transfer enhancement in a mini-channel with hydrophobic and hydrophilic patterns, International Journal of Heat and Mass Transfer, 68 (2014) 151-160.
[25] B. Peng, X. Ma, Z. Lan, W. Xu, R. Wen, Experimental investigation on steam condensation heat transfer enhancement with vertically patterned hydrophobic–hydrophilic hybrid surfaces, International Journal of Heat and Mass Transfer, 83 (2015) 27-38.
[26] X. Ji, D. Zhou, C. Dai, J. Xu, Dropwise condensation heat transfer on superhydrophilic-hydrophobic network hybrid surface, International Journal of Heat and Mass Transfer, 132 (2019) 52-67.
[27] J. Lee, S. Lee, J. Lee, Improved humid air condensation heat transfer through promoting condensate drainage on vertically stripe patterned bi-philic surfaces, International Journal of Heat and Mass Transfer, 160 (2020) 120206.
[28] J. Xie, Q. She, J. Xu, C. Liang, W. Li, Mixed dropwise-filmwise condensation heat transfer on biphilic surface, International Journal of Heat and Mass Transfer, 150 (2020) 119273.
[29] J. Yuan, Y. Wang, J. Xu, X. Ji, J. Xie, Convective dropwise condensation heat transfer in mini-channels with biphilic surface, International Journal of Heat and Mass Transfer, 134 (2019) 69-84.
[30] J. Xie, J. Xu, Q. Liu, X. Li, Coupling diffusion welding technique and mesh screen creates heterogeneous metal surface for droplets array, Advanced Materials Interfaces, 4(23) (2017) 1700684.
[31] P.S. Mahapatra, A. Ghosh, R. Ganguly, C.M. Megaridis, Key design and operating parameters for enhancing dropwise condensation through wettability patterning, International Journal of Heat and Mass Transfer, 92 (2016) 877-883.
[32] B. Mondal, M. Mac Giolla Eain, Q. Xu, V.M. Egan, J. Punch, A.M. Lyons, Design and fabrication of a hybrid superhydrophobic–hydrophilic surface that exhibits stable dropwise condensation, ACS Applied Materials & Interfaces, 7(42) (2015) 23575-23588.
[33] Y. Zhu, C. Tso, T. Ho, M.K. Leung, S. Yao, H. Qiu, Heat transfer enhancement on tube surfaces with biphilic nanomorphology, Applied Thermal Engineering, 180 (2020) 115778.
[34] Y. Zhu, C.Y. Tso, T.C. Ho, M.K. Leung, S. Yao, Coalescence-Induced Jumping Droplets on Nanostructured Biphilic Surfaces with Contact Electrification Effects, ACS Applied Materials & Interfaces, 13(9) (2021) 11470-11479.
[35] K.K. Varanasi, M. Hsu, N. Bhate, W. Yang, T. Deng, Spatial control in the heterogeneous nucleation of water, Applied Physics Letters, 95(9) (2009) 094101.
[36] X. Chen, J. Wu, R. Ma, M. Hua, N. Koratkar, S. Yao, Z. Wang, Nanograssed micropyramidal architectures for continuous dropwise condensation, Advanced Functional Materials, 21(24) (2011) 4617-4623.
[37] Y. Hou, M. Yu, X. Chen, Z. Wang, S. Yao, Recurrent filmwise and dropwise condensation on a beetle mimetic surface, ACS Nano, 9(1) (2015) 71-81.

[38] Y. Zheng, C.-H. Chen, H. Pearlman, R. Bonner, Enhanced Filmwise Condensation With Thin Porous Coating, in: First Pacific Rim Thermal Engineering Conference (PRTEC), Big Island, HI, Paper No. PRTEC-14728, 2016.
[39] R. Wang, D.S. Antao, Capillary-enhanced filmwise condensation in porous media, Langmuir, 34(46) (2018) 13855-13863.
[40] D.J. Preston, K.L. Wilke, Z. Lu, S.S. Cruz, Y. Zhao, L.L. Becerra, E.N. Wang, Gravitationally driven wicking for enhanced condensation heat transfer, Langmuir, 34(15) (2018) 4658-4664.
[41] J. Oh, R. Zhang, P.P. Shetty, J.A. Krogstad, P.V. Braun, N. Miljkovic, Thin film condensation on nanostructured surfaces, Advanced Functional Materials, 28(16) (2018) 1707000.
[42] B. Shirani, T. Kaghazchi, M. Beheshti, Water and mercaptan adsorption on 13X zeolite in natural gas purification process, Korean Journal of Chemical Engineering, 27(1) (2010) 253-260.
[43] D. Tchernev, Solar energy application of natural zeolites, Natural zeolites: Occurrence, properties, use, 474 (1978) 485.
[44] M.K.I. Khan, M.A. Schutyser, K. Schroën, R.M. Boom, Electrostatic powder coating of foods–State of the art and opportunities, Journal of Food Engineering, 111(1) (2012) 1-5.
[45] K.C. Chan, C.Y. Chao, C. Wu, Measurement of properties and performance prediction of the new MWCNT-embedded zeolite 13X/CaCl2 composite adsorbents, International Journal of Heat and Mass Transfer, 89 (2015) 308-319.
[46] K.C. Chan, C.Y.H. Chao, G.N. Sze-To, K.S. Hui, Performance predictions for a new zeolite 13X/CaCl2 composite adsorbent for adsorption cooling systems, International Journal of Heat and Mass Transfer, 55(11-12) (2012) 3214-3224.
[47] I.A. Larmour, S.E. Bell, G.C. Saunders, Remarkably simple fabrication of superhydrophobic surfaces using electroless galvanic deposition, Angewandte Chemie International Edition, 46(10) (2007) 1710-1712.
[48] D. Chung, Materials for thermal conduction, Applied Thermal Engineering, 21(16) (2001) 1593-1605.
[49] L. Zhu, C. Tso, K. Chan, C. Wu, J. Chen, W. He, S. Luo, C.Y. Chao, Performance investigation of nanostructured composite surfaces for use in adsorption cooling systems with a mass recovery cycle, Science and Technology for the Built Environment, 24(10) (2018) 1084-1103.
[50] B. Traipattanakul, C.Y. Tso, C.Y. Chao, Electrostatic-induced coalescing-jumping droplets on nanostructured superhydrophobic surfaces, International Journal of Heat and Mass Transfer, 128 (2019) 550-561.
[51] A.G. Bailey, The science and technology of electrostatic powder spraying, transport and coating, Journal of Electrostatics, 45(2) (1998) 85-120.
[52] A. Ghosh, S. Beaini, B.J. Zhang, R. Ganguly, C.M. Megaridis, Enhancing dropwise condensation through bioinspired wettability patterning, Langmuir, 30(43) (2014) 13103-13115.
[53] T.L. Bergman, F.P. Incropera, D.P. DeWitt, A.S. Lavine, Fundamentals of Heat and Mass Transfer, John Wiley & Sons, 2011.
[54] W. Alnaser, A. Barakat, Use of condensed water vapour from the atmosphere for irrigation in Bahrain, Applied Energy, 65(1-4) (2000) 3-18.
[55] H.K. Observatory, Climatological Information Services, in, https://www.hko.gov.hk/en/cis/climat.htm, 2021.
[56] D. Or, Scaling of capillary, gravity and viscous forces affecting flow morphology in unsaturated porous media, Advances in Water Resources, 31(9) (2008) 1129-1136.

[57] B. Majhy, R. Iqbal, A. Sen, Facile fabrication and mechanistic understanding of a transparent reversible superhydrophobic–superhydrophilic surface, Scientific Reports, 8(1) (2018) 1-11.

Appendix A

Appendix B

Click here to access/download

Supplementary Material

Appendix B. Supplementary materials_video.mp4